Computational Analysis for the Combination of Inductive Coupled Wireless Coils and High Permittivity Materials to Improve B1 Field for Rhesus Monkey MRI

Daniel Hernandez and Kyoung-Nam Kim

Department of Biomedical Engineering
Gachon University, Incheon, Korea
theasdwmove@gmail.com, kn16.kim@gmail.com

Abstract ─ Magnetic resonance imaging (MRI) scanning of small animals such as non-human primates has been of interest in recent years. Imaging primates, such as rhesus monkeys, presents challenges due to the shape of their head. The shape and dimensions of the head can cause poor magnetic flux density ($|B_1|$) strength and penetration to specific regions of interest. In this study, we focus on the design of an eight-channel, helmet-style array coil for rhesus monkey brain imaging, and performed quantitative analysis by means of electromagnetic (EM) simulations and acquiring reception sensitivity ($|B_1^-|$)-fields to demonstrate that the use of combining inductively coupled wireless coils and high permittivity materials can improve the $|B_1^-|$-field sensitivity of a tradition phase array coil.

Index Terms ─ EM simulations, high permittivity materials, MRI RF coils, small animals, wireless coil.

I. INTRODUCTION

Rhesus monkey brain scanning with magnetic resonance imaging (MRI) is a useful method to study brain anatomy, functionality, and reactions to new drugs; these discoveries are intended to be transferable to human applications due to the similarities between primates [1]. Although anatomically and physiologically the brains of monkeys and humans share some similarities, imaging monkey brains requires dedicated hardware to accommodate the smaller size of their head and different structure of their body. Especial frames needs to be constructed to keep the monkey in an optimal and stationary position of the body and head inside the scanner during MR imaging. Given that the frontal facial area of the monkey is more pronounced than the human nose, it is necessary to tailor the dimensions of the radio-frequency (RF) coil. The use of traditional birdcage coils would fail to deliver a uniform field due to the different distances between the head and the coil in the upper and lower nasal areas. It has been reported that by using a birdcage coil positioned only around the upper area of the monkey's head it is possible to maintain a uniform field in the brain area [2]. However, this required a macaque monkey to be seated in a sphinx-like manner, with a frame used to restrain the monkey's movement, and performed while the monkey was sedated. A single transmit/receive (Tx/Rx) coil configuration was a standard approach taken to imaging conscious monkeys, since it is easy to setup and can be used with any size of monkey; however, in terms of imaging quality its performance was low. One study proposed a combination of a single 100 mm loop coil for transmission and a phase array coil of four channels for the reception coil [3]; this configuration was used to perform functional MRI (fMRI) and diffusion MRI on a monkey. Another novel proposal was the use of a traveling wave system as the Tx method by attaching a two-port patch antenna to the RF shield of the gradient system of the MRI scanner; the antenna produced a TE_{11} mode generating a circular polarized (CP) magnetic flux density ($|B_1|$)-distribution, while for reception a three-element phase array (PA) coil was used, but this configuration only covered the upper half of a cylinder around a monkey's brain [4]. The use of PA loop coils as receptors for MRI is common practice due to their simplicity and capacity to produce high sensitivity $|B_1|$-field, in addition to being able to perform parallel imaging (PI) [5], and thus reducing scan time. The use of helmet style PA loop array coils [6, 7] is common for its increase reception field sensitivity.

There is ongoing research into an optimal coil configuration and geometry that would produce a higher signal intensity and uniform $|B_1|$-field [8] for small animals such as rhesus monkeys. One potential coil configuration that has been proposed in recent years is the use of inductive coupled wireless (w_L) coils; these elements have been shown to enhance the imaging performance of standard PA coil by producing stronger and more uniform $|B_1|$-fields [9]. The operation of the w_L coils consists on generating a magnetic field from induced currents. The induced currents on the w_L come from pick up varying $|B_1|$-fields produced from the

Submitted On: June 11, 2019
Accepted On: September 7, 2019

standard PA coil with active current sources. In this coil configuration, the $|B_1|$-field intensity can be increased.

It has also been reported that the use of high-permittivity material (HPM) attachments can increase the magnetic field [10-12]. The HPM operate as a focusing material that will help increase the efficiency of the $|B_1|$-field, especially at high frequencies such as the ones used in high field MRI. Previous studies have shown that the use of HPM enhance the $|B_1|$-field strength, improving the signal-to-noise ratio (SNR) and the image quality overall. The HPM have been proposed as a simple and low-cost accessory to increase the performance of traditional PA coil.

In the present study we propose a receive only helmet-style PA coil for use with rhesus monkey brain imaging at 7T, by using a combination of wireless coils and HPM attachments, to enhance the sensitivity of the $|B_1^-|$-field produced by a traditional PA coil. We performed a quantitative analysis by using electromagnetic (EM) simulations to acquire $|B_1|$-field maps of the standard PA coil and the proposed combination with w_L coil and HPM attachments.

II. METHODS

A. Loop array coil design

The proposed receive only helmet-style PA coil is composed of eight loop coils that are distributed to fit around the shape of the head of a rhesus monkey. The PA coil array consists of two loop coils located at the front and back of the monkey head model, this coils will be referenced as anterior-posterior (AP) coils and two coils at each lateral side. The active coils (standard PA coil) are located close to the imaging object, as an inner layer, while the w_L array coils are located at the same position as the active coil but in an outer layer separated by 15 mm. Figure 1 shows the dimensions for each type of coil, the active and wireless coil for the AP and lateral locations in the array, in addition to the HPM materials corresponding to each set of coils.

Table 1 summarize the dimensions of each of the coils and the HPM. There is a slight curvature at top of each of the coils and HPM to cover the shape of the monkey head model. The AP active and w_L coils are smaller than the lateral coil, but their top and bottom width are same. The PA coils are placed near the monkey's head to receive a stronger $|B_1|$-field sensitivity, and in order to increase the sensitivity a w_L coil array was also attached as an outer layer to the active receive array.

In addition to the w_L coils, an arrangement of eight HPM attachments were inserted between the active and w_L coils. The HPM attachments had similar geometry to the coils shape, their dimensions are also listed in Table 1, and the geometry is show in Fig 1 (c).

Table 1: The dimensions of active and wireless coils and the HPM

	Height [mm]	Width [mm] Top/Bottom	Thickness [mm]
AP active coil (Fig. 1 (a))	40	20/30	0.5
AP w_L coil (Fig. 1 (a))	50	26/45	0.5
AP HPM (Fig. 1 (c))	40	23/35	5.0
Lat. Active coil (Fig. 1 (b))	80	20/30	0.5
Lat. w_L coil (Fig. 1 (b))	100	26/45	0.5
Lat. HPM (Fig. 1 (c))	90	23/35	5.0

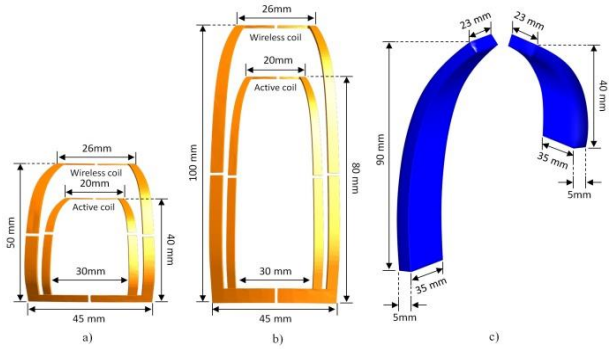

Fig. 1. Dimensions for the loop coils, with the active coils in the inner layer and the wireless coil in the outer layer, for (a) anterior and posterior (AP) coils, (b) lateral coils, and (c) the high permittivity material (HPM).

Figure 2 shows the combinations used in this study, as reference evaluation we will use the standard PA coil or active coil only (inner layer of coils), as can be visualized in Figs. 2 (a), (d) for the *xz*- and *xy*-plane views. The inner layer of eight loop coils was placed around a 33 mm radius circumference for the top of each coil. The first evaluation condition was the use of w_L coils as shown in Figs. 2 (a), (d), arranged in an outer layer of 42 mm of radius. The second evaluation condition was the use of the standard PA coil and the w_L with the HPM attachments (Figs. 2 (b), (e)). A model of a rhesus monkey is included with the array coil (Figs. 2 (c), (f)).

The three-dimensional (3D) model of a monkey head was computed by taking multiple coronal 2-D MRI images of a rhesus monkey head. The MR images were combined to form a 3D volume image. The voxeling was done with Photoshop (Adobe Inc, California 95110, USA) and it was rendered using Rhinoceros 3D modeling tools (McNeel, Seattle, WA, USA). The measured size

of the monkey was 86 × 125 × 105 mm, while the rhesus monkey head model has dimensions of 81.7 × 118.8 × 104.7 mm^3. Organ segmentation was excluded in modeling process, which makes the phantom solid, for this reason the electrical properties of the phantom were set to a continuous value.

The w_L coils were tuned to operate at the desired frequency of 300 MHz corresponding to a 7T MRI system, and matched to 50 Ohms. There was a frequency shift from the tuning condition when the HPM attachments were added, the frequency shift was on average 1.4 MHz between individual coils; for this reason, it was necessary to repeat the tuning of the w_L coil. The w_L coils are not connected with a current source as they operate with the currents induced by the active coils.

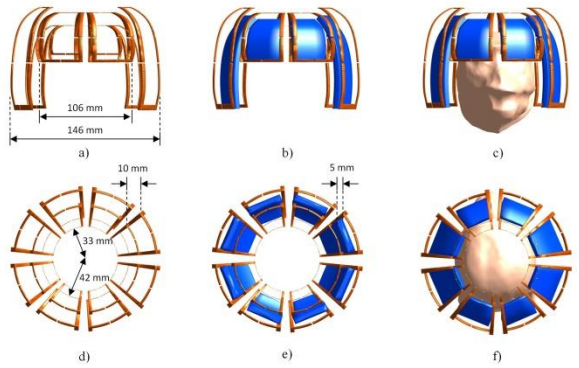

Fig. 2. View of the arrangement of the array coil, for the xz-plane (top) and the xy-plane (bottom). (a), (d): the active and wireless coils; (b), (e): the array with the high permittivity attachments; (c), (f): the array coil fitting the rhesus monkey phantom.

III. RESULTS

By means of electromagnetic (EM) simulations we designed and acquired reception sensitivity ($|B_1^-|$)-fields on a mimicked rhesus monkey phantom, with electrical properties of 0.413 S•m^{-1} and 43.77, conductivity and permittivity respectively. The electrical properties for the monkey phantom were selected to represent brain white matter, and the values were used as provided by the data base in the simulation software. The electrical values used in this work are similar to the human brain white matter, given that there's no information of the conductivity and permittivity of rhesus monkey brain at 300 MHz. however, these values fit well towards the goal of this work, which is to show the benefits of using wireless coils and HPM to increase the $|B_1^-|$-field. A dedicated study should be done such as [13] to compute the electrical properties of the rhesus monkey brain. In addition the focus of pre-clinical animal MRI research is to translate the technology to human applications, therefore the use of human brain electrical properties values are within our objective. The phantom model has an homogeneous filling because it was acquired by 3D scanning the surface of the monkey head, for this reason a single value of electrical properties were used. The HPM attachments were designed to emulate barium titanate ($BaTiO_3$), which has electrical properties of 300 permittivity and 0.5 S•m^{-1} conductivity [14, 15]. The simulations were performed using the commercial FDTD software, Sim4life (Zurich MedTech AG (ZMT)).

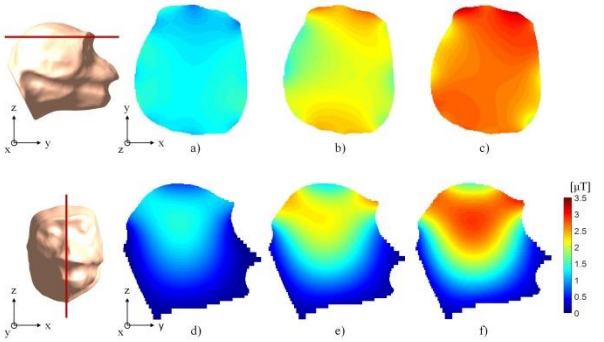

Fig. 3. The $|B_1^-|$-fields for two different slices from an axial view (top row) and sagittal view (bottom row). (a), (d): active array coil only; (b), (e): with the wireless coil; (c), (f): the combination of the wireless coil and HPM.

Figure 3 shows the $|B_1^-|$-field in the axial (*xy*)- and sagittal (*yz*)-slice for the reference active coil (Figs. 3 (a), (d)). The $|B_1^-|$-field resulting of the combination of the active and w_L coils are shown in Figs. 3 (b), (e), and the $|B_1^-|$-field from the combination of the active PA coil with w_L coils and the HPM attachments is shown in Figs. 3 (c), (f). The red arrows on the monkey's head model indicate the position of the slices taken for the figure. The average and normalized standard deviation values of each $|B_1^-|$-field for the whole slice are shown in Table 2.

Table 2: Statistical values for the $|B_1^-|$-field acquired using different coil configurations

	Average [μT]			**Standard Deviation [μT]**		
View	**Active**	**Active + w_L**	**Active +w_L +HPM**	**Active**	**Active + w_L**	**Active +w_L +HPM**
Slice #1	1.14	2.00	2.60	0.047	0.039	0.051
Slice # 2	0.96	1.90	2.50	0.100	0.065	0.061
Sagittal	0.56	1.02	2.32	0.152	0.240	0.300

Electrical ($|E|$)-fields were also acquired to understand the effect of the proposed combinations used in this study. Figures 4 (a), (d) show the $|E|$-field of the active coil for axial and sagittal slice. For the axial slice the average value was 51.09 and 2.91 V•m^{-1} of standard deviation. Figures 4 (b), (e) show the combination of the active coil and the w_L coil, with an average and standard deviation of 81.8 and 4.16 V•m^{-1} respectively, for the

axial slice. Lastly, the |E|-fields for the combination of the active PA coil with w_L coil and HPM attachments are show in Figs. 4 (c), (f), with average and standard deviation 102.1 and 4.58 V•m^{-1} respectively.

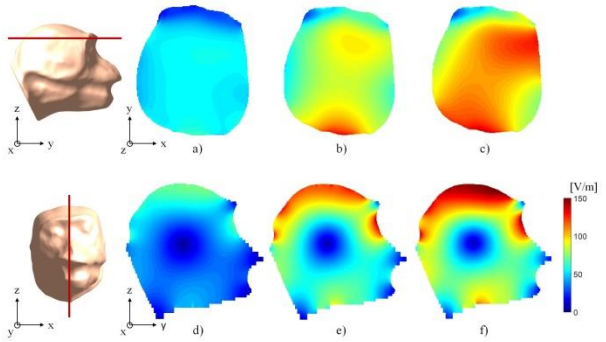

Fig. 4. The |E|-field for the axial view (top row) and sagittal view (bottom row) for (a), (d): only the active array coil; (b), (e): with the wireless coil; (c), (f): the combination of the wireless coil and HPM.

IV. CONCLUSION

The results from the simulation indicate the potential of the proposed combination of w_L coils and HPM attachments to improve the $|B_1^-|$-field of the traditional PA coil. On average, the $|B_1^-|$-field sensitivity was increased almost two times in comparison with the reference PA array coil only. The proposed receive only coil configuration could be a promising method for imaging small animals such as rhesus monkeys.

ACKNOWLEDGMENT

This research was supported by a grant (HO16C0004) from Osong Innovation Center, funded by the Ministry of Health & Welfare, the Republic of Korea.

REFERENCES

[1] S. Hofer, K. D. Merboldt, R. Tammer, and J. Frahm, "Rhesus monkey and human share a similar topography of the corpus callosum as revealed by diffusion tensor MRI in vivo," *Cerebral Cortex*, vol. 18, no. (5), pp. 1079-1084. 2007.

[2] C. A. Roopnariane, Y. C. Ryu, M. R. Tofighi, P. A. Miller, S. Oh, J. Wang, B. S. Park, L. Ansel, C. A. Lieu, T. Subramanian, and Q. X. Yang, "Quadrature RF coil for in Vivo brain MRI of a macaque monkey in a stereotaxic head frame," *Concepts Magn. Reson. Part B*, vol. 41, no. 1, pp. 22, 2012.

[3] M. H. Khachaturian, "A 4-channel 3 Tesla phased array receive coil for awake rhesus monkey fMRI and diffusion MRI experiments," *J. Biomed. Sci. Eng.*, vol. 3, no. 11, pp. 1085, 2010.

[4] T. Herrmann, J. Mallow, M. Plaumann, M. Luchtmann, J. Stadler, J. Mylius, M. Brosch, and J. Bernarding, "The travelling-wave primate system: A new solution for magnetic resonance imaging of macaque monkeys at 7 Tesla ultra-high field," *PloS One*, vol. 10, no. 6, 2015.

[5] M. A. Ohliger, and D. K. Sodickson, "An introduction to coil array design for parallel MRI," *NMR Biomed*., vol. 19, no. 3, pp. 300, 2006.

[6] M. Perez, D. Hernandez, E. Michel, M. H. Cho, and S. Y. Lee. "A tool box to evaluate the phased array coil performance using retrospective 3D coil modeling" *J. Korean Soc. Magn. Reson. Med.*, vol. 18, no. 2, pp. 107. 2014.

[7] B. Keil, J. N. Blau, S. Biber, P. Hoecht, V. Tountcheva, K. Setsompop, C. Triantafyllou, and L. L. Wald, "A 64- channel 3T array coil for accelerated brain MRI," *Magn. Reson. Med.*, vol. 70, pp. 248, 2013.

[8] J. R. Hadley, C. M. Furse, and D. Parker, "RF coil design for MRI using a genetic algorithm," *Applied Computational Electromagnetics Society Journal*, vol. 22, no. 2, pp. 277, 2007.

[9] M. Bilgen, "Inductively-overcoupled coil design for high resolution magnetic resonance imaging," *Biomedical Engineering Online*, vol. 5, no. 1, pp. 3, 2006.

[10] J. H. Seo, S. D. Han, and K. N. Kim, "Improvements in magnetic field intensity and uniformity for small-animal MRI through a high-permittivity material attachment," *Electron. Lett.*, vol. 52, no. 11, pp. 898, 2016.

[11] J. H. F. van Gemert, W. M. Brink, A. G. Webb, and R. F. Remis, "Designing high-permittivity pads for dielectric shimming in MRI using model order reduction and Gauss-Newton optimization," *ICEAA*, pp. 417. 2017.

[12] W. M. Teeuwisse, W. M. Brink, and A. G. Webb, "Quantitative assessment of the effects of high-permittivity pads in 7 Tesla MRI of the brain," *Magn. Reson. Med.*, vol. 67, no. 5, pp. 1285, 2012.

[13] L. Hao, L. Xu, B. Yang, and G. Li, "Image reconstruction based on the anatomical information for magnetic resonance electrical impedance tomography," *Applied Computational Electromagnetics Society Journal*, vol. 31, no. 6, 2016.

[14] N. S. Panwar and B. S. Semwal, "Study of electrical conductivity of barium titanate ceramics," *Ferroelectrics*, vol. 115, pp. 1, 1991.

[15] W. M. Teeuwisse, W. M. Brink, K. N. Haines, and A. G. Webb, "Simulations of high permittivity materials for 7 T neuroimaging and evaluation of a new barium titanate-based dielectric," *Magn. Reson. Med*., vol. 67, no. 4, pp. 912, 2012.